CHAPTER 5
POOL BOILING HEAT TRANSFER ON VERTICAL MINI-FINNED SURFACES IN SATURATED FC-72

The heat transfer performance and associated flow pattern observation for pool boiling of dielectric fluid FC-72 on finned surfaces in a vertical orientation are examined in this chapter. In this part of study, the FC-72 boiling temperature is also set at 56.6℃ corresponding to the saturated pressure 1 atm. The measured boiling incipience superheat, boiling heat transfer coefficient, and CHF value are presented in terms of the geometric parameters. Moreover, comparison of the effect of orientation on boiling heat transfer performance is also conducted.

5.1 Flow Pattern Observation

For a finned surface at vertical orientation, fin spacing and fin length significantly affect the interaction of the wake and thermal boundary layers of each fin. The cooling fluid towards the finned surface is stable, but the leaving fluid showed a large fluctuation because of the disturbances induced while passing the fin array. Moreover, bubble generation, growth and departure mechanism on horizontal fin of vertical finned surface are complex with three different surfaces which including upward-facing surface, vertical surface, and downward-facing surface. Hence, the optical observation of the bubbly flow pattern is carried out in this study for comparison with geometric parameter effects on boiling heat transfer performance.

The flow patterns for saturated dielectric fluid FC-72 boiling on finned surface on a vertical orientation are observed and displayed in Figures 5.1 to 5.4. The progression of pooling boiling of flow patterns with increasing the heat flux are from 4×10^{3} Wm^{-2} to 8×10^{5} Wm^{-2}.

At the beginning of the experiment, free convection is the dominant heat transfer mechanism until the wall superheat exceeds the incipience boiling temperature. Figure 5.1 shows the flow patterns of initial boiling on 12 various finned surfaces. The figures

demonstrate that most bubbles are grow from the downward-facing surface of the horizontal fins which due to the cooling liquid to be obstructed by horizontal fins and formed stagnant condition under the downward-facing surface of each fin. Therefore, the thermal boundary layer on the downward-facing surface is thicker than that of other facing surfaces and wall superheat here is also relatively larger. Moreover, it is clearly observed that the movement of bubbles is clearly constrained by the horizontal fins. In particular, the bubbles generated from the downward-facing surface of fins gradually grow or coalesce with other bubbles until they blanket the entire downward-facing surface and reach the edge of fin, then separate and slip to lift-off along the vertical fin spacing.

The boiling flow patterns at low heat flux region are showed in Figure 5.2. It is found that bubbles become larger and depart at higher frequency. Figure 5.2 (a) and (b) show, for smaller fin spacing surfaces, bubbles would attach the upward-facing surface of next lower row fins before grow to a certain diameter equivalent to the fin width. It might decrease the bubble growth/departure period because of the increase in the heating area. Besides, Figure 5.2 (a), (e) and (i) also show that for the lowest fin length surfaces, some bubbles grow to over the fin tip before they grow to larger than the fin width and then depart from the fin tip and lift-off without any obstruction. This indicates that low profile fins (fin length lower than fin width) make bubbles to depart easier and thus attain higher departure frequency. Moreover, the sliding bubbles along the vertical fin spacing to impact the upper fins are also investigated in each test surface. The mechanism for bubbles to impact fins would activates more nucleate sites and render bubbles trapped or re-accumulated with bubbles on the downward-facing surface of upper fins. Furthermore, in Figure 5.2 (b), (c) and (d), the deformed bubbles along the vertical fin spacing are also investigated. This observation can be ascribed to the fact that bubbles interact and merge each other in smaller fin spacing. On the contrary, in Figure 5.2 (i), (j), (k) and (l), flow patterns on larger fin spacing surfaces exhibit a different phenomenon in which bubbles generated from adjacent fins slip upward without other interaction.

In moderate heat flux region, as shown in Figure 5.3, the boiling area spreads to entire heated surface and most of the fins accumulate the bubbles at their downward-facing surface. In Figure 5.3 (b), (c) and (d), vapor columns are observed to slip along the vertical fin spacing. This is the result of more many bubbles generated and violent bubble interaction between closer fin spacing. Moreover, small vapor mushrooms are observed in the fin tip on smaller fin spacing surfaces, especially with high fin length as seen from Figure 5.3 (c) and (d). Vapor columns along the vertical fin spacing and vapor mushrooms on fin tip indicate that smaller spacing induce larger flow resistance for bubble departure and expanding bubbles out the fin array. By contrast, in larger spacing surface as shown in Figure 5.3 (i), (j), (k) and (l), bubbles departing from adjacent fins still do not interact.

In the high heat flux regime approaching CHF, as shown in Figure 5.4, rapid and violent vapor behaviors are investigated on all tested surface. Figure 5.4 (a), (e), and (i) show flow patterns on the surfaces with lower fin length. Those test surfaces exhibit a similar vapor behavior that being completely covered with a thick vapor layer. Another significant vapor behavior is observed on the surfaces with high fin length as shown in Figure 5.4 (b), (c), and (d). It is clearly noted that vapor mushrooms expand out the top and the perimeter of fin array due to the large flow resistance to vapor cloud in closer fin spacing (S=0.5mm). Similar behavior is also observed in Figure 5.4 (f), (g) and (h) that test surfaces with fin spacing of 1mm. By contrast, flow pattern observed on larger-spacing finned surface as shown in Figure 5.4 (j), (k) and (l)) shows a different vapor behavior in which vapor clouds can travel along the vertical fin spacing without any expanding. It is suggested that vapor mushrooms blanket the heating surface result the heat transfer mechanism become the relatively ineffective conduction through the vapor mushroom and induce the rapid rise in wall temperature.

5.2 The Effects of the Geometric Parameter on Boiling Heat Transfer Performance

5.2.1 Boiling Incipience Superheat and CHF

The experimental results of boiling incipience superheat, temperature excursion and CHF values are plotted in the boiling curves in Figures 5.5 to 5.7. It is noted that on finned surfaces the boiling incipience superheat and temperature excursion are relatively small and insignificant. Comparing to plain surface, the flow motion on finned surface is much more complicated and violent due to the fact that horizontal fins obstruct the cooling flow. The flow stagnant under the downward-facing surface of horizontal fins might induce the lower boiling incipience superheat and temperature excursion. The stagnant flow here results thicker thermal boundary layer and higher wall superheat. Moreover, Table5.1 indicates that the smaller the fin spacing, the lower the boiling incipience superheat. Similar behavior is also observed by Xia et al. [29]. By contrast, the data also show that the longer the fin length, the smaller the boiling incipience superheat. The reason for low incipience superheat is that the fluid is obstructed by fins and provided higher energy in order to initiate the boiling.

To be more specific on how the geometric parameters affect the CHF, Table 5.2 show the enhancement factor of the CHF ($q''_{b,CHF}/q''_{p,CHF}$) for various geometric parameters. The experimental results present the enhancement factor of CHF decrease with the increase in fin length and also the decrease with the fin spacing. In the previous discussion of boiling flow patterns at high heat flux region, vapor mushrooms out the fin array are observed on denser and higher finned surface. This is considered that higher fin length and closer fin spacing produce larger flow resistance which in turn obstructs vapor mushrooms leaving from and re-wetting liquid entering the finned surface can result lower heat transfer rate.

The values of CHF ($q''_{b,CHF}$) with different structure geometry parameters including fin spacing and fin length are plotted in Figure 5.8. The data show the CHF values increase with the fin length and decrease in fin spacing. This can be ascribed to the fact that denser and higher fin array can provide more wetting area and also higher heat transfer rate. Moreover, the plot shows the effect of fin length on CHF value is more significant than that of the fin spacing.

For example, although both test surfaces (S=1.0mm, L=4mm) and (S=0.5mm, L=2.0mm) have almost 1.5 times area to the test surface (S=1.0mm, L=2.0mm), however, the CHF value of the test surface (S=1.0mm, L=4.0mm) is about 28% higher than that test surface (S=0.5mm, L=2.0mm).

The enhanced heat transfer ratio ($\dot{Q}_{f,CHF} / \dot{Q}_{p,CHF}$) versus the area ratio (A_t / A_b) is plotted in Figure 5.9. Similar to the horizontal arrangement, the figure shows that $\dot{Q}_{f,CHF} / \dot{Q}_{p,CHF}$ increases with A_t / A_b as increasing the area increases the heat transfer. However, the plot also showed that $\dot{Q}_{f,CHF} / \dot{Q}_{p,CHF}$ is linear proportional to A_t / A_b until A_t / A_b>5. As area ratio A_t / A_b>5, enhanced heat transfer ratio $\dot{Q}_{f,CHF} / \dot{Q}_{p,CHF}$ begin to decay. Compared with Figure 4.16, it is found that $\dot{Q}_{f,CHF} / \dot{Q}_{p,CHF}$ of vertical finned surface is larger than that of horizontal arrangement. Figure 5.9 also depicts $q''_{f,CHF} / q''_{p,CHF}$ against A_t / A_b. It shows two distinct regions of enhancements - A_t / A_b<5 and A_t / A_b>5. Those results also prove the flow pattern observation that lower aspect ratio fins with either lower fin length or larger fin spacing provide lower resistance to the departure bubbles and re-wetting liquid and yield higher heat transfer rate per unit area in vertical orientation.

In the previous discussion in the chapter 4, the dimensionless quantity (S/L) significant affects the CHF behavior on horizontal mini-finned surfaces. For analyzing the effect of surface structure including fin length and fin spacing on CHF, the vertical mini-finned surfaces' CHF values that based on overall surface area are normalized by vertical plain surface's CHF value and are plotted in Figure 5.10 to illustrate CHF behavior. The normalized CHF values ($q''_{t,CHF} / q''_{p,CHF}$) is also observed raised with increase in dimensionless quantity (S/L). However, unlike the plot of the horizontal mini-finned surfaces, a peak value of 1.35 is found in the S/L=2. Moreover, most normalized CHF values in the high (S/L) region of 1 to 4 become

relatively constant with values of 1.3. This indicates that rarer fins and shorter extended fin of the vertical mini-finned surfaces might be enhanced the hydrodynamic mechanisms of departing bubble and re-wetting liquid. The normalized CHF data in Figure 5.10 is correlated by curve fitting:

$$q''_{t,CHF} / q''_{p,CHF} = 1.8 - 0.568(\frac{S}{L})^{-0.293} \quad (5\text{-}1)$$

5.2.2 Boiling Heat Transfer Coefficient on Vertical Mini-Finned Surfaces

The effects of the geometry parameter of vertical finned surfaces on saturated boiling heat transfer coefficient of FC-72 are examined. The measured experimental data are presented in Figure 5.11 to 5.14 to illustrate the relationship of the boiling heat transfer coefficient with heat flux for various fin length and fin spacing. The increase in boiling heat transfer coefficient is ascribed to high nucleation density on heating surface, higher bubble generation frequency and faster bubble growth while increasing the heat flux. The result data also show that reduce the fin spacing can get better boiling heat transfer coefficient in low and moderate heat flux region. The buoyancy force pushes the bubbles upward against the flow resistance of horizontal fins on the finned surface. This mechanism thus augments the convection contribution to heat transfer by increasing the liquid's velocity inside the fin spacing. Thus closer fin spacing can induce stronger convection to enhance heat transfer on finned surface. At high heat fluxes, however, denser finned surfaces tend to perform poorer because closer fins spacing obstructs the vapor/bubbles leaving from and also the re-wetting liquid entering the finned surface. In addition, Kim et al. [30] observed that the vapor movement was enhanced by the spacing structure as the heating surface is downward facing. Hwang et al. [28] and Xia et al. [29] reported closer narrow channel width could enhance the boiling heat transfer coefficient in low heat flux region. Moreover, as shown in Figure 5.12 to 5.14, the plots illustrate that the heat transfer coefficient increases noticeably with heat flux until a peak value then shows significant

decline at high heat flux region. This can be ascribed to the fact that larger vapor mushrooms blanket the surface and thus induce large rise in wall superheat at high heat flux region. However, as shown in Figure 5.11, the boiling heat transfer coefficient shows a different trend at high heat flux region in which the boiling heat transfer coefficient does not change evidently with heat flux. Base on the photographic analysis of the boiling on higher finned surface, it can be concluded that no significant change in flow/vapor departure mechanism on surface with high fin length from moderate to high heat flux. Moreover, early decay in boiling heat transfer coefficient for denser finned surface is observed for different fin length. The plots also show that denser finned surface has better heat transfer coefficient than rarer arrangement prior to the peak value. However, the trend reverses after the peak value and denser fin surface result in lower heat transfer coefficient.

It is also note that all curves in Figure 5.11, to 5.14 have almost the same trend of the overall heat transfer coefficients in low heat flux region. Figure 5.15 re-plots the overall heat transfer coefficients versus the overall heat flux for twelve test surfaces that before the maximum points. Figure 5.15 shows that all experimental data lie on a straight line which can be correlated in a linear equation form:

$$h_t = 11.393 q_t''^{0.559} \tag{5-2}$$

Eq. (5-2) can also be written in term of the power law:

$$q_t'' = 249 \Delta T^{2.267} \tag{5-3}$$

which evidences the dependence on the wall superheat. The exponent appears in Eq. (5-3) is close to that which appears in Rohsenow's correlation [55] for nucleate boiling.

5.3 Orientation Effect on Mini-Finned Surfaces

The comparisons of boiling incipience superheat between horizontal and vertical orientation are listed in Table 4.1 and 5.1 respectively. One can clearly observe that the boiling

incipience superheat for the vertical arrangement is rather small. Similar observations were reported by Guglielmini et al. [9] for their experimental study associated with HT-55 dielectric fluid.

The boiling curves in which overall heat transfer coefficient versus heat flux of finned surfaces with horizontal and vertical orientations are illustrated in Figure 5.16 to 5.19. For a smaller fin length and fin spacing of 0.5mm as shown in Figure 5.16, there is a negligible difference of nucleate boiling for the range of $q_t'' < 50000$ Wm^{-2}. As $q_t'' > 50000$ Wm^{-2}, one can see a significant difference that the vertical finned surface contributes slightly higher boiling heat transfer coefficient. As seen in Figure 5.17, as the fin length is increased to 4.0 mm while the fin spacing is still kept at 0.5mm, the boiling heat transfer coefficient for vertical arrangement is superior to that of horizontal arrangement. This is associated with interaction and accumulation of rising bubbles between closer transverse spacing, causing strong fluid flow back to the fin array and inducing bubbles and flow out of the vertical spacing. As shown in Figures 5.16, the boiling heat transfer coefficient is distinct between vertical and horizontal orientation when the heat flux is high. A further increase of overall heat flux over 1.2×10^5 Wm^{-2} for L=0.5mm and 7×10^4 Wm^{-2} for L=4.0mm, one can see a drop of boiling coefficient for the vertical arrangement. This phenomenon can be explained from the flow patterns of Figure 5.3(a) and (b). For the vertical arrangement having a prescribed high heat flux operated at a small fin spacing of 0.5mm, the generated vapor between vertical directions is relatively difficult to be freed from their nucleation sites.

Conversely, for a larger fin spacing of 2.0mm as shown in Figure 5.18and Figure 5.19 and the flow patterns of Figure 5.3(i) and (l), the generated vapor is comparatively easy to be removed from the vertical position, thereby leading to no detectable difference of heat transfer performance provided that $q_t'' < 1.5\times10^5$ Wm^{-2}. Moreover, the boiling heat transfer performance for horizontal orientation apparently outperforms that of vertical arrangement when $q_t'' > 1.5\times10^5$ Wm^{-2}. The results are different from those of a smaller fin spacing of

0.5mm in which an enhanced performance is observed in high heat flux region. The reason is that the distance between adjacent fins is large so that it is hard to cause the flow disturbance and interaction/coalescence of bubbles. In summary, one can see a significant improvement of boiling performance on finned surfaces with smaller fin spacing on vertical arrangement.

5.4 Conclusion Remarks

The experimental investigations of pool boiling phenomena for the vertical finned surfaces immersed in saturated FC-72 at atmospheric pressure are presented in this study. The effects of geometry parameters with different fin length and spacing on the nucleate boiling heat transfer performance are also reported. Analysis of the experimental results leads to the following conclusions:

1. The departure and lift-off of bubbles for vertical finned surfaces are different from the horizontal ones. Most of the initial bubbles are generated from the downward-facing surface of horizontal fins on vertical base surfaces. The bubbles grow or accumulate to a certain size larger than fin width, separate at fin edge, slip along the fin spacing and then lift-off.
2. The extended fins of vertical heating surface will become a real obstacle to upward motion of bubbles. At very low heat fluxes, there are only a few isolated bubbles. As heat flux increases, the bubbles coalescence and rise more rapidly. Approaching to the moderate heat flux region, the accumulated bubbles is observed in more compact finned surfaces and the re-wetting liquid become hardly from entering the fin array.
3. The boiling incipience superheat and temperature excursion on vertical finned surfaces are smaller and unapparent because the extended fins can induce thick thermal boundary layer on their downward-facing surface and result early boiling initiation.
4. Closer fin spacing and higher fin length provide higher heat transfer area per unit base area and therefore better heat transfer rate. The test results also show that enhancement in heat

transfer rate by increasing fin length which is more significant than by reducing the fin spacing.

5. The narrower fin spacing can obstruct the re-wetting liquid with the result to increase in heat transfer coefficient at low heat flux region due to the disturbance in thermal boundary layer. However, at high heat flux region, the horizontal fins obstruct the vapor mushrooms from the heating surface and might decrease in boiling heat transfer coefficients.
6. The orientation effect on boiling performance is sensitive to the smaller fin spacing arrangement. For the finned surface with smaller fin length and fin spacing, there is a negligible difference of nucleate boiling at low heat flux region. But there are higher boiling heat transfer coefficients on vertical orientation at high heat flux region. For the finned surface with larger fin length and smaller fin spacing, the boiling heat transfer performance for vertical configuration is superior to that of horizontal arrangement.
7. The nucleate boiling and CHF performance of the finned surface at horizontal orientation is found to be slightly better than that of the finned surface at vertical orientation for the present finned surface geometry and may be due to the vertical orientation having a significant portion of the finned surface area facing downward.

Table 5.1 Average boiling incipience superheat of mini-finned surfaces.

Boiling Incipience Superheat (K)	L=0.5mm	L=1.0mm	L=2.0mm	L=4.0mm
S=0.5mm	4.85	3.59	3.18	2.65
S=1.0mm	6.24	5.11	4.48	3.31
S=2.0mm	7.30	6.06	5.24	4.08

Table 5.2 Enhancement factor of CHF for various mini-finned surfaces.

$q''_{b,CHF}$ / $q''_{p,CHF}$	L=0.5mm	L=1.0mm	L=2.0mm	L=4.0mm
S=0.5mm	2.31	3.19	4.24	6.39
S=1.0mm	2.04	2.52	3.36	5.43
S=2.0mm	1.69	2.21	3.03	4.51

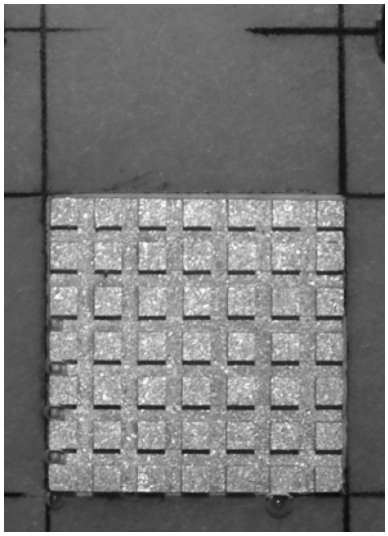

(a) S=0.5mm, L =0.5mm, 1.2% of CHF

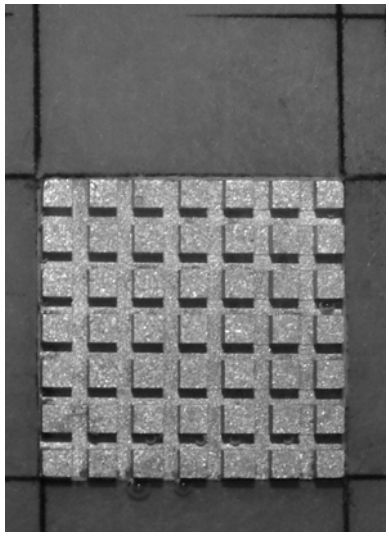

(b) S=0.5mm, L =1.0mm, 1.0% of CHF

g

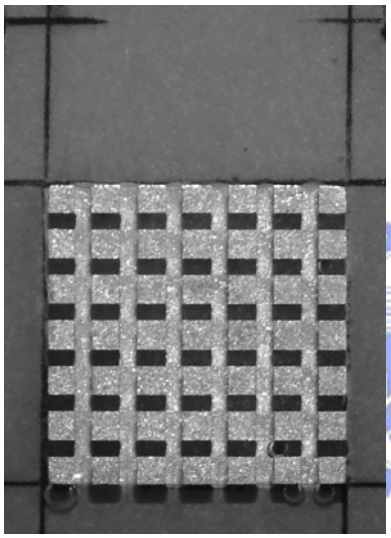

(c) S=0.5mm, L =2.0mm, 0.7% of CHF

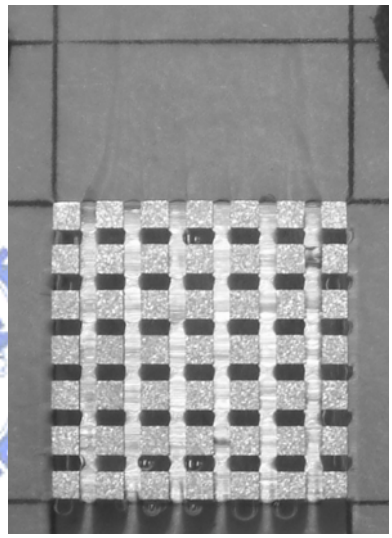

(d) S=0.5mm, L =4.0mm, 0.5% of CHF

g

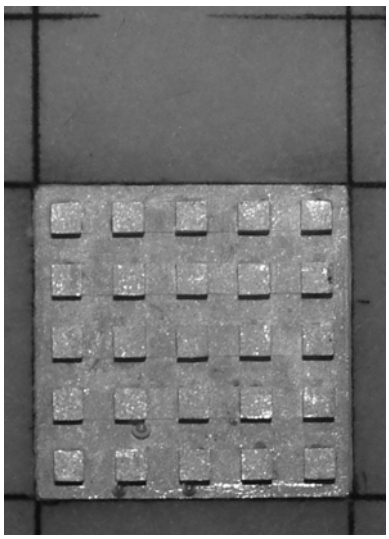

(e) S=1.0mm, L =0.5mm, 1.4% of CHF

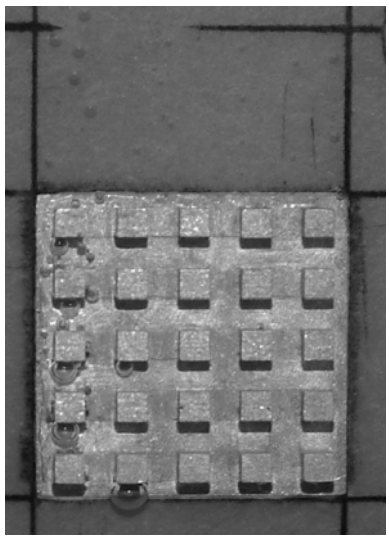

(f) S=1.0mm, L =1.0mm, 1.6% of CHF

g

Figure 5.1 Flow patterns of 12 mini-finned surfaces at boiling incipience.

continued

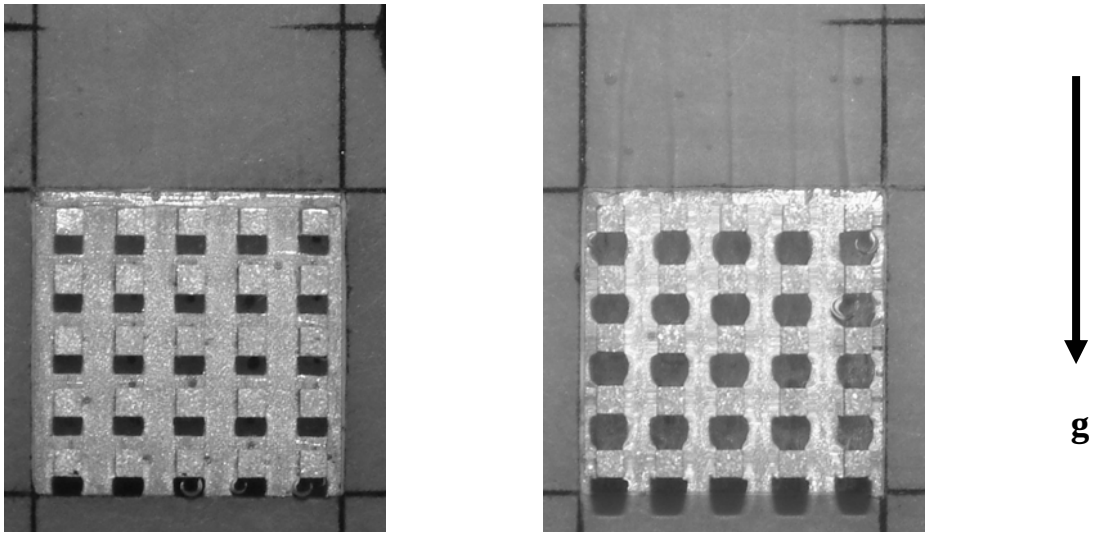

(g) S=1.0mm, L =2.0mm, 1.0% of CHF (h) S=1.0mm, L =4.0mm, 0.7% of CHF

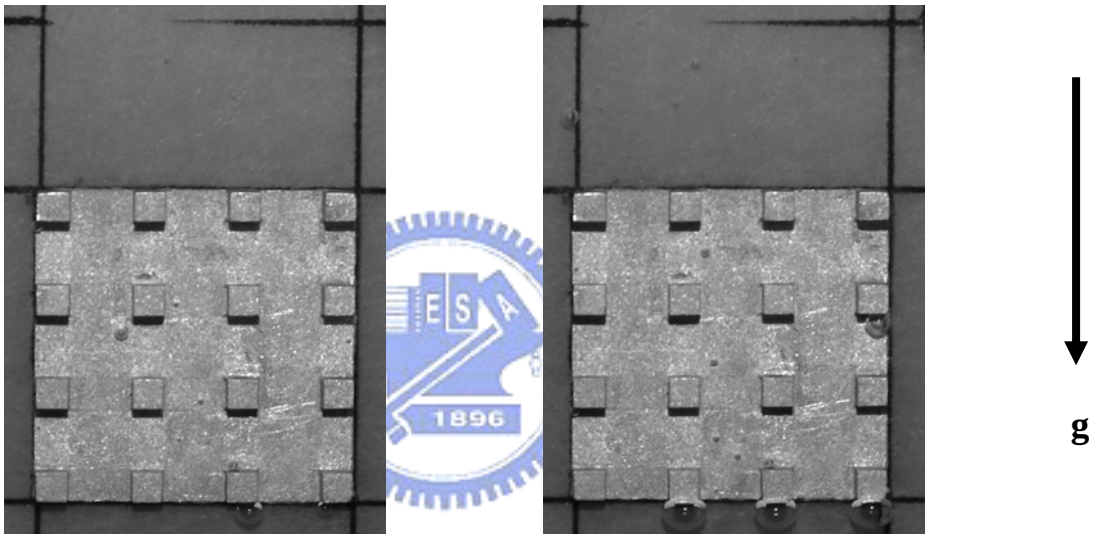

(i) S=0.5mm, L =4.0mm, 1.7% of CHF (j) S=1.0mm, L =1.0mm, 1.3% of CHF

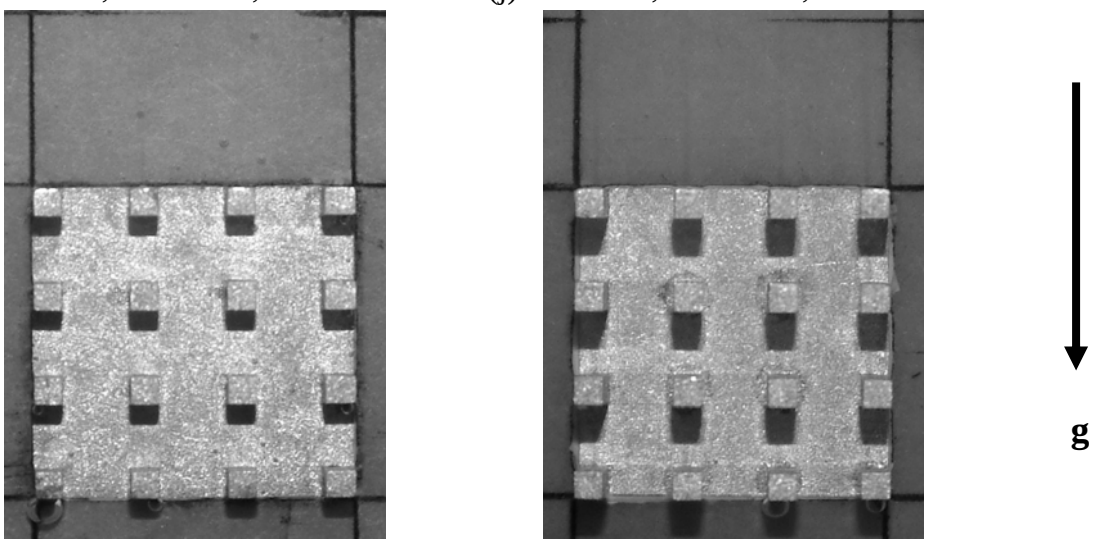

(k) S=0.5mm, L =2.0mm, 1.0% of CHF (l) S=1.0mm, L =4.0mm, 0.8% of CHF

Figure 5.1 Flow patterns of 12 mini-finned surfaces at boiling incipience.

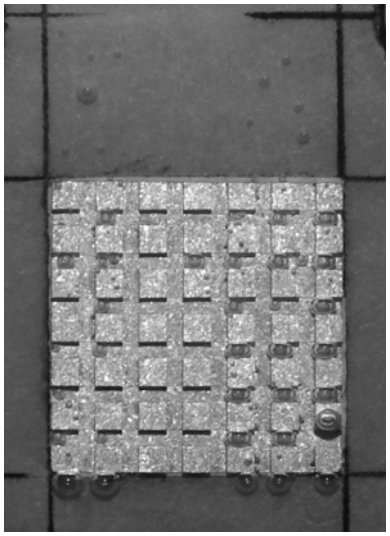

(a) S=0.5mm, L =0.5mm, 20.6% of CHF

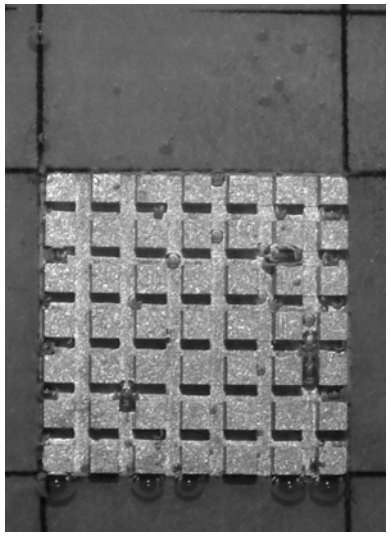

(b) S=0.5mm, L =1.0mm, 22.9% of CHF

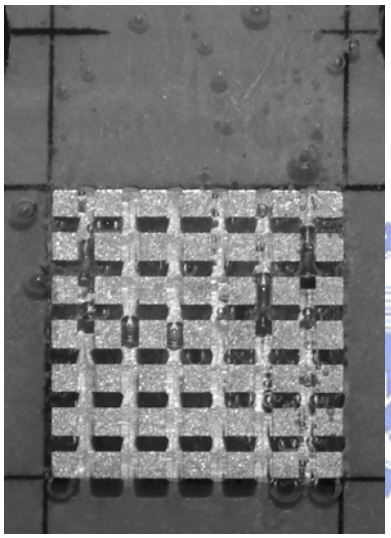

(c) S=0.5mm, L =2.0mm, 22.3% of CHF

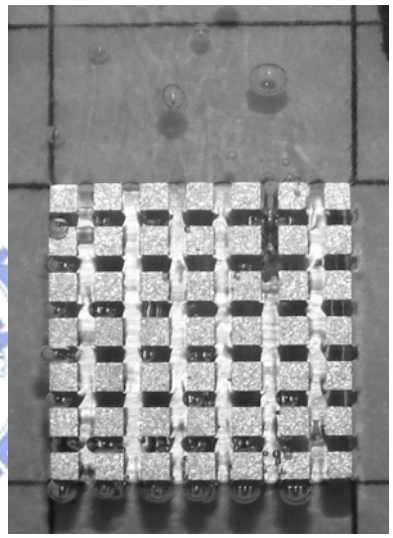

(d) S=0.5mm, L =4.0mm, 21.5% of CHF

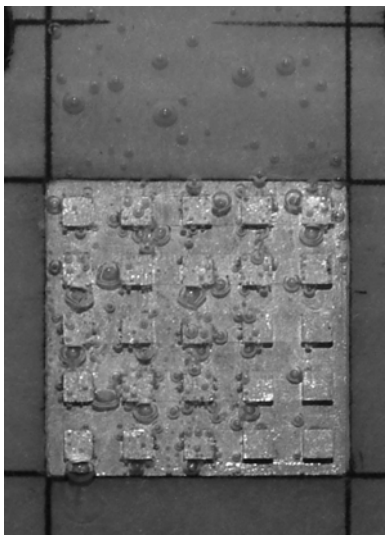

(e) S=1.0mm, L =0.5mm, 22.7% of CHF

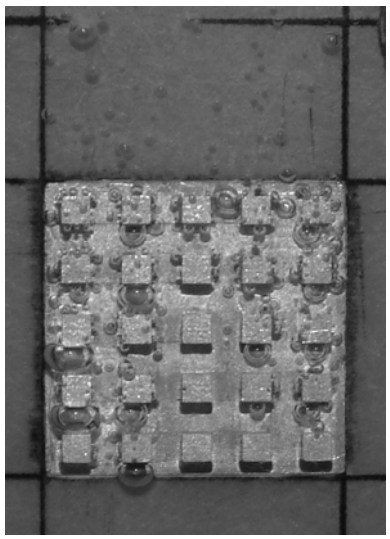

(f) S=1.0mm, L =1.0mm, 20.8% of CHF

g

g

g

Figure 5.2 Flow patterns of 12 mini-finned surfaces at low heat flux region.

continued

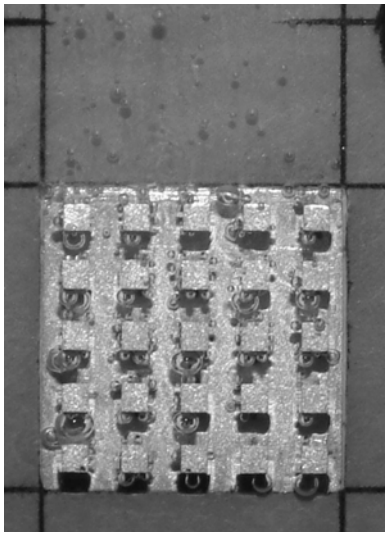

(g) S=1.0mm, L =2.0mm, 22.2% of CHF

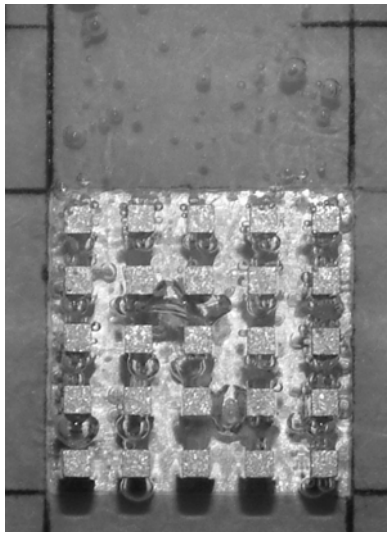

(h) S=1.0mm, L =4.0mm, 23.4% of CHF

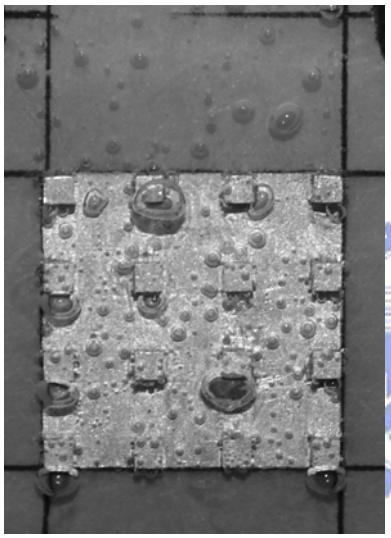

(i) S=2.0mm, L =0.5mm, 22.8% of CHF

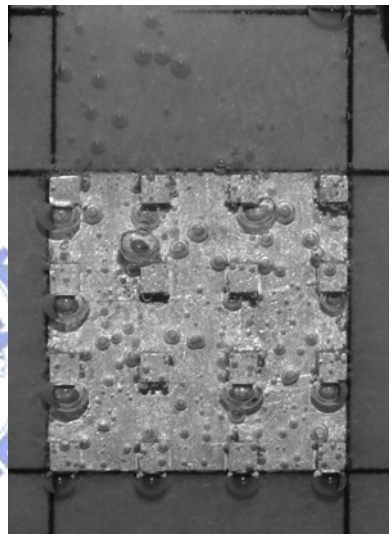

(j) S=2.0mm, L =1.0mm, 23.8% of CHF

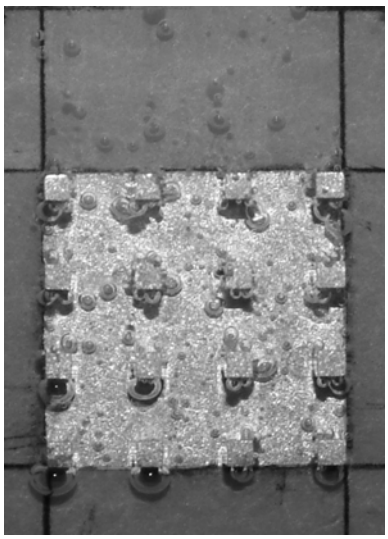

(k) S=2.0mm, L =2.0mm, 21.1% of CHF

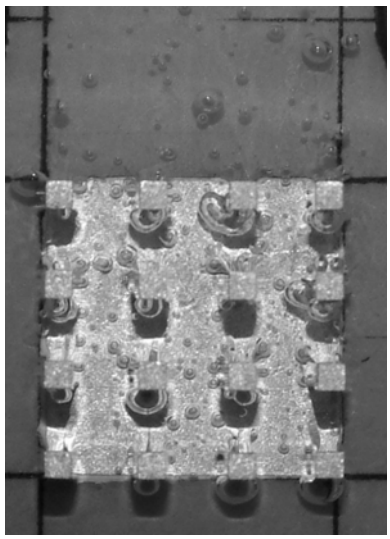

(l) S=2.0mm, L =4.0mm, 20.3% of CHF

Figure 5.2 Flow patterns of 12 mini-finned surfaces at low heat flux region.

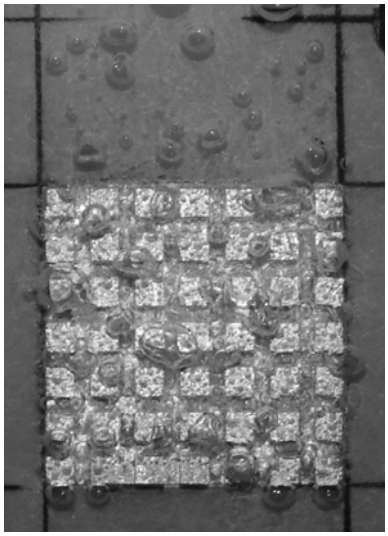

(a) S=0.5mm, L =0.5mm, 54.6% of CHF

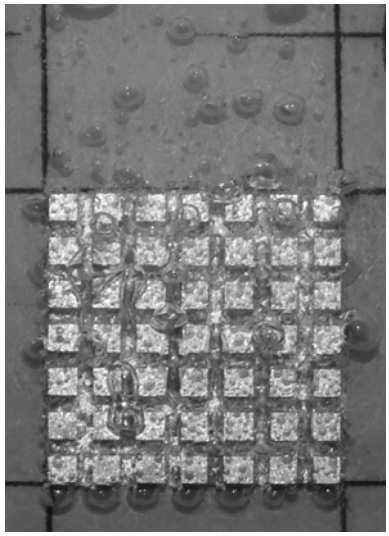

(b) S=0.5mm, L =1.0mm, 53.9% of CHF

g

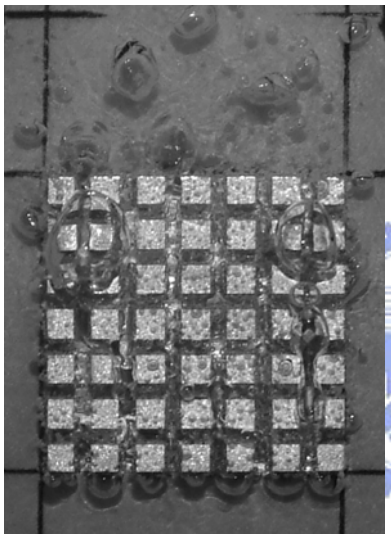

(c) S=0.5mm, L =2.0mm, 52.3% of CHF

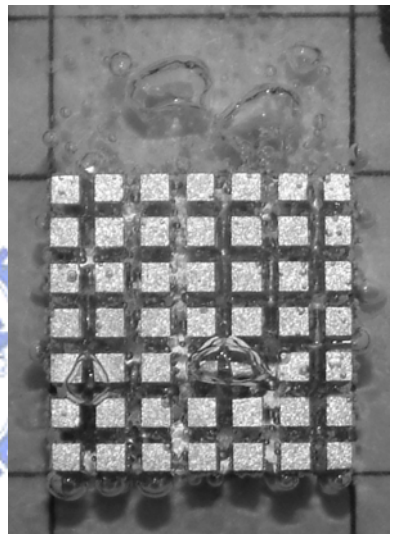

(d) S=0.5mm, L =4.0mm, 55.6% of CHF

g

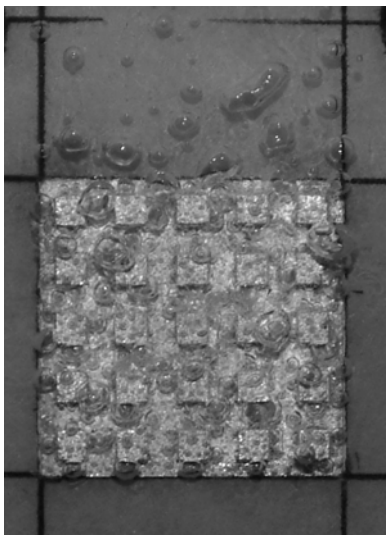

(e) S=0.5mm, L =0.5mm, 55.3% of CHF

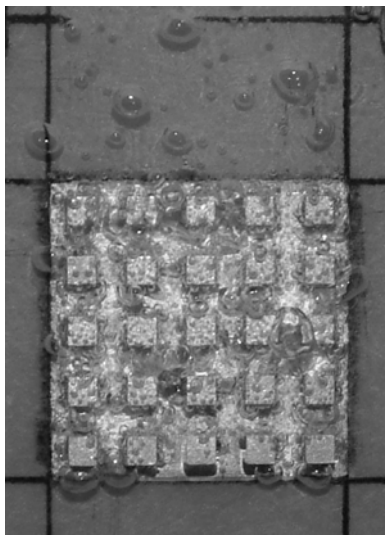

(f) S=0.5mm, L =1.0mm, 53.4% of CHF

g

Figure 5.3 Flow patterns of 12 mini-finned surfaces at moderate heat flux region. continued

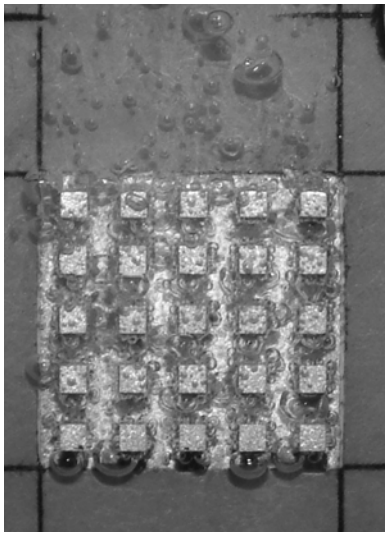

(g) S=1.0mm, L =2.0mm, 54.5% of CHF

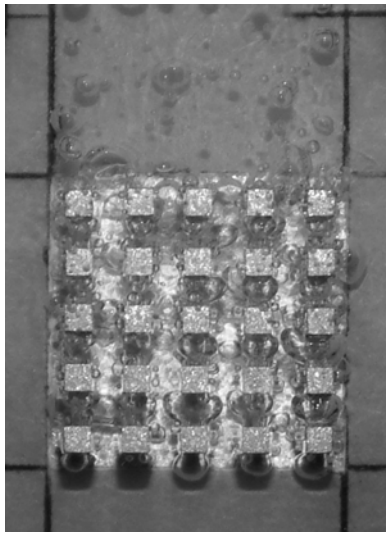

(h) S=1.0mm, L =4.0mm, 54.9% of CHF

g

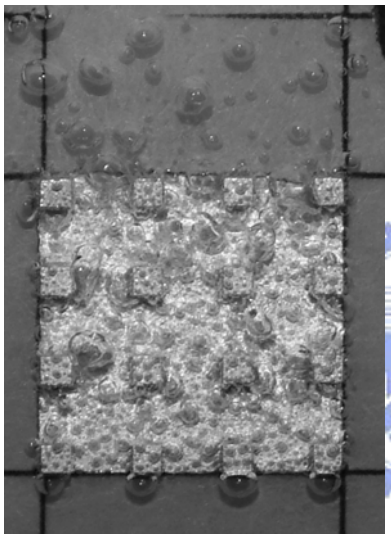

(i) S=0.5mm, L =0.5mm, 52.9% of CHF

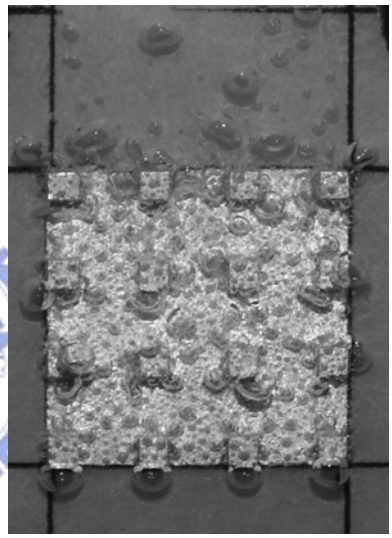

(j) S=0.5mm, L =1.0mm, 54.8% of CHF

g

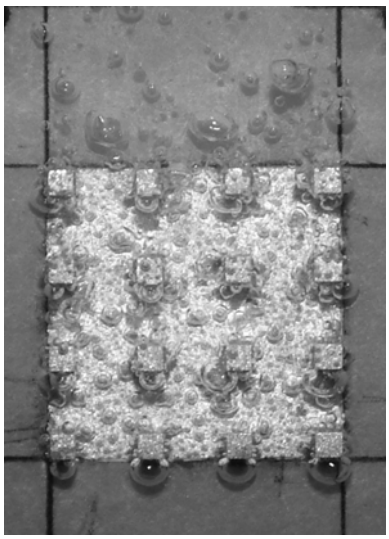

(k) S=2.0mm, L =2.0mm, 55.2% of CHF

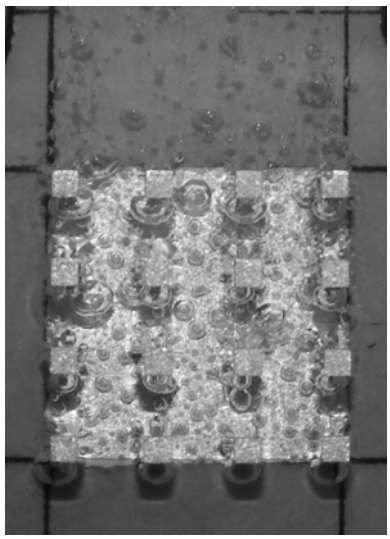

(l) S=2.0mm, L =4.0mm, 54.7% of CHF

g

Figure 5.3 Flow patterns of 12 mini-finned surfaces at moderate heat flux region.

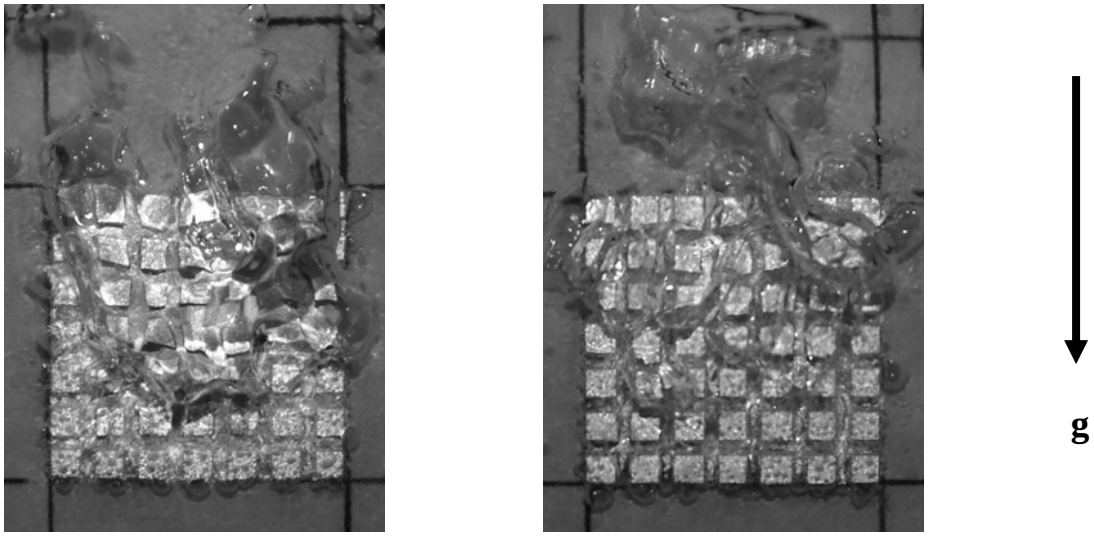

(a) S=0.5mm, L =0.5mm, 87.8% of CHF (b) S=0.5mm, L =1.0mm, 86.3% of CHF

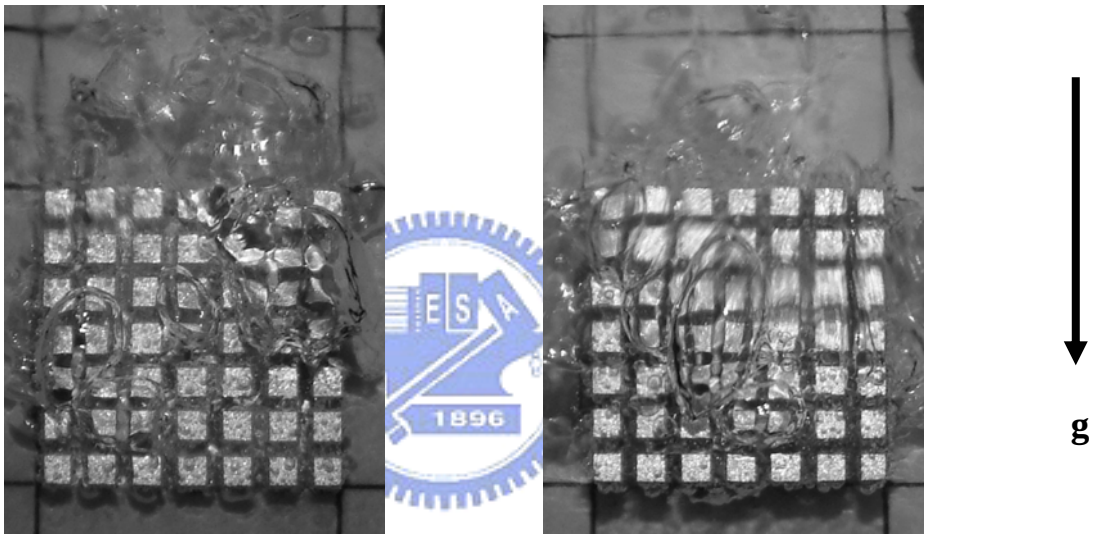

(c) S=0.5mm, L =2.0mm, 88.0% of CHF (d) S=0.5mm, L =4.0mm, 87.1% of CHF

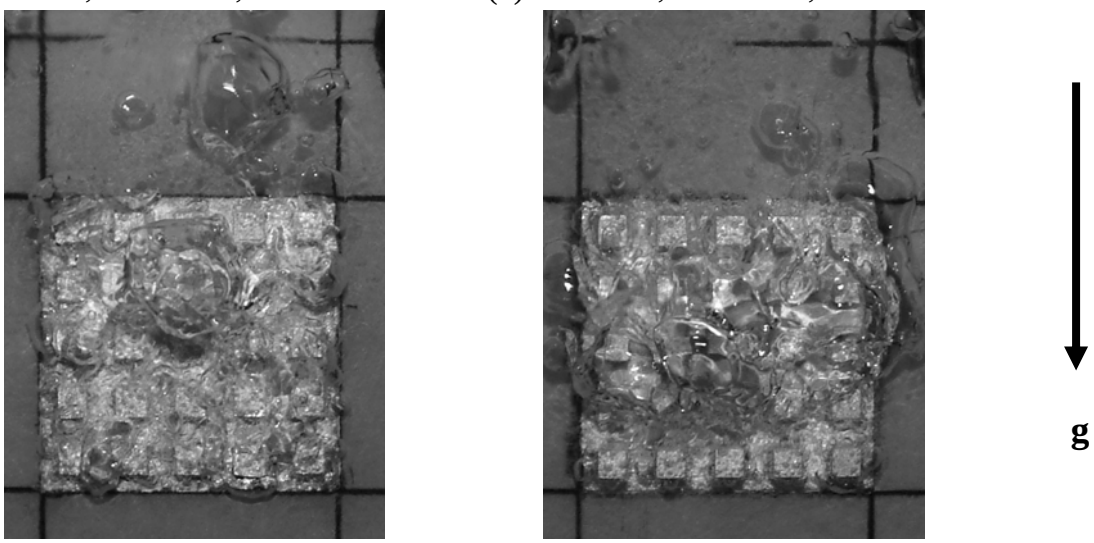

(e) S=1.0mm, L =0.5mm, 88.5% of CHF (f) S=1.0mm, L =1.0mm, 89.1% of CHF

Figure 5.4 Flow patterns of 12 mini-finned surfaces at high heat flux region. continued

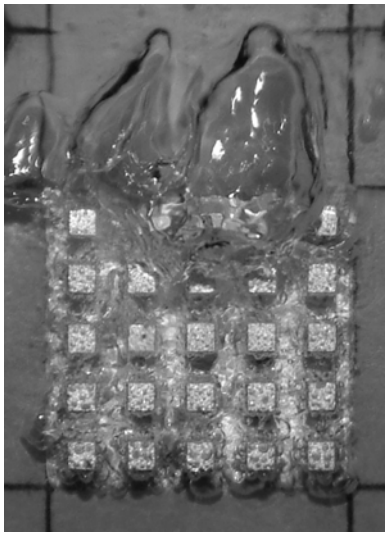

g

(g) S=1.0mm, L =2.0mm, 88.9% of CHF (h) S=1.0mm, L =4.0mm, 89.4% of CHF

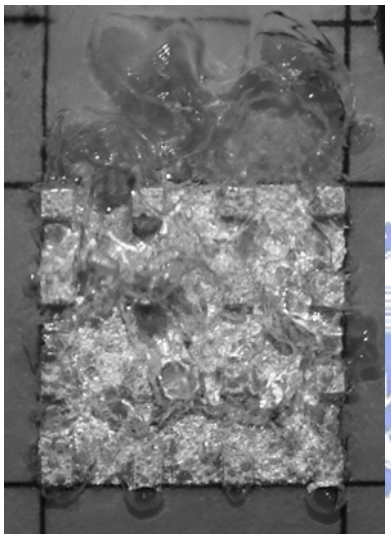

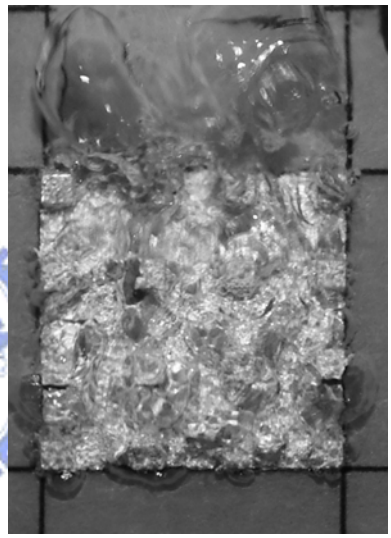

g

(i) S=2.0mm, L =0.5mm, 88.1% of CHF (j) S=2.0mm, L=1.0mm, 87.3% of CHF

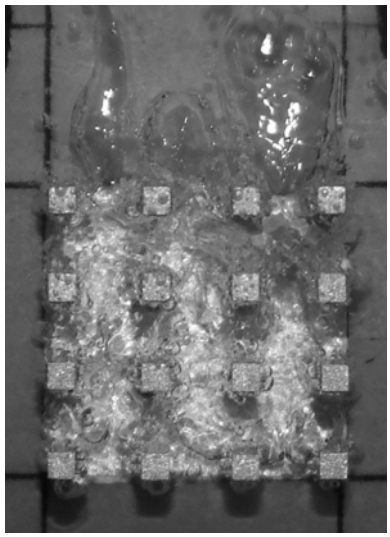

g

(k) S=2.0mm, L=2.0mm, 89.6% of CHF (l) S=2.0mm, L =4.0mm, 88.2% of CHF

Figure 5.4 Flow patterns of 12 mini-finned surfaces at high heat flux region.

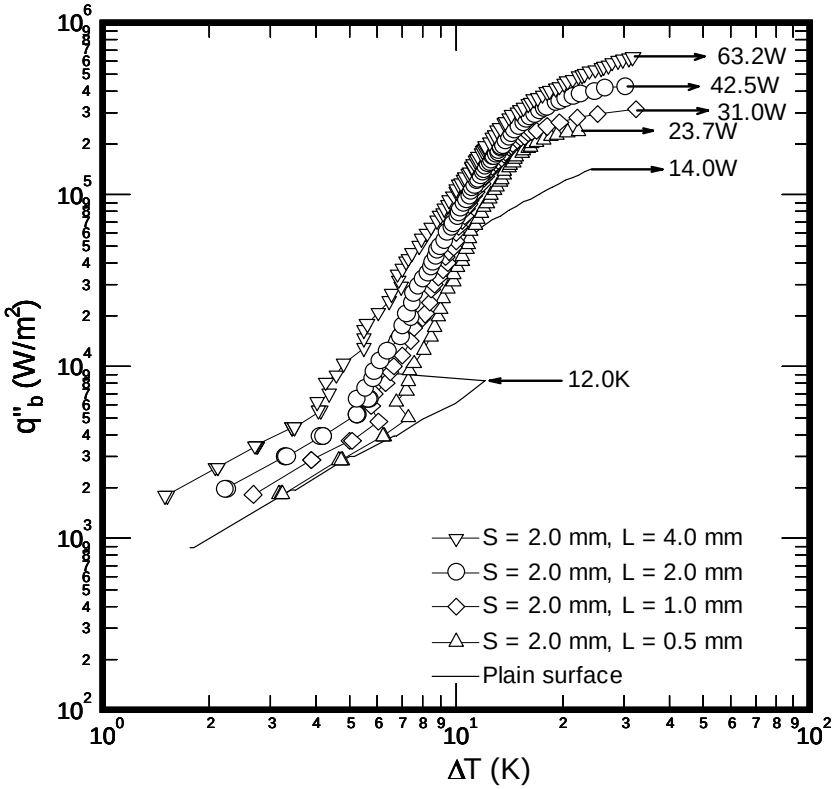

Figure 5.5 Boiling curves of mini-finned surface in vertical orientation (S=2.0mm, increasing heat flux).

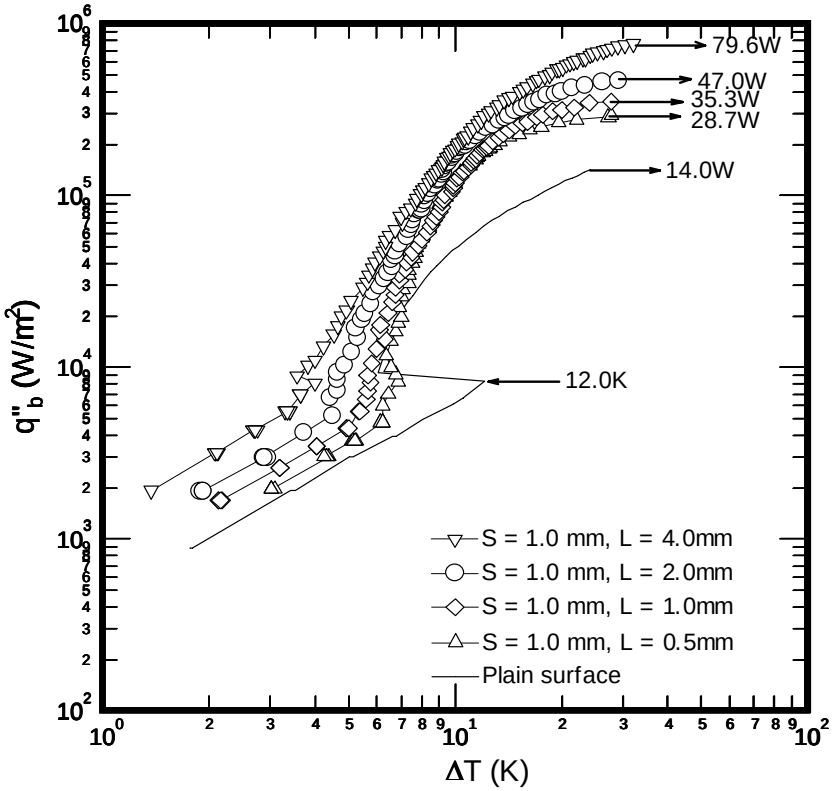

Figure 5.6 Boiling curves of mini-finned surface in vertical orientation (S=1.0mm, increasing heat flux).

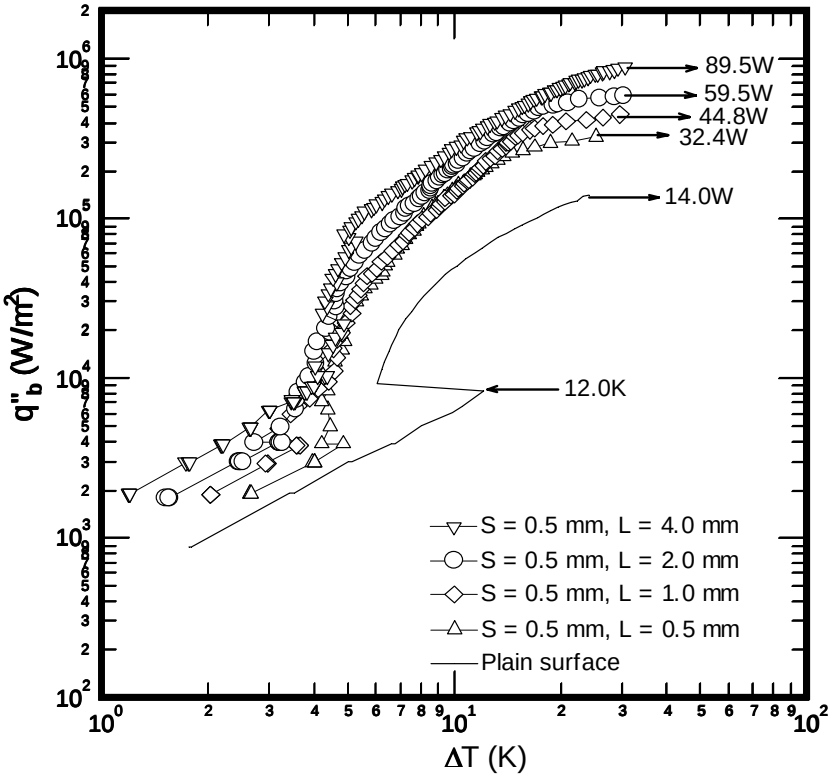

Figure 5.7 Boiling curves of mini-finned surface in vertical orientation (S=0.5mm, increasing heat flux).

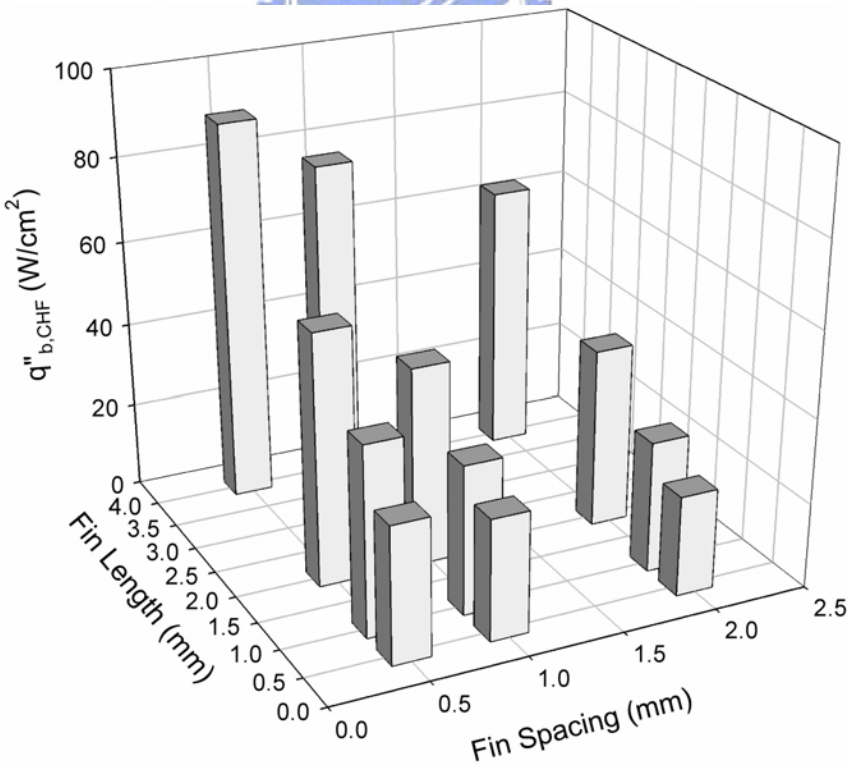

Figure 5.8 Critical heat flux ($q''_{b,CHF}$) varied with fin length and fin spacing of mini-finned surfaces in vertical orientation..

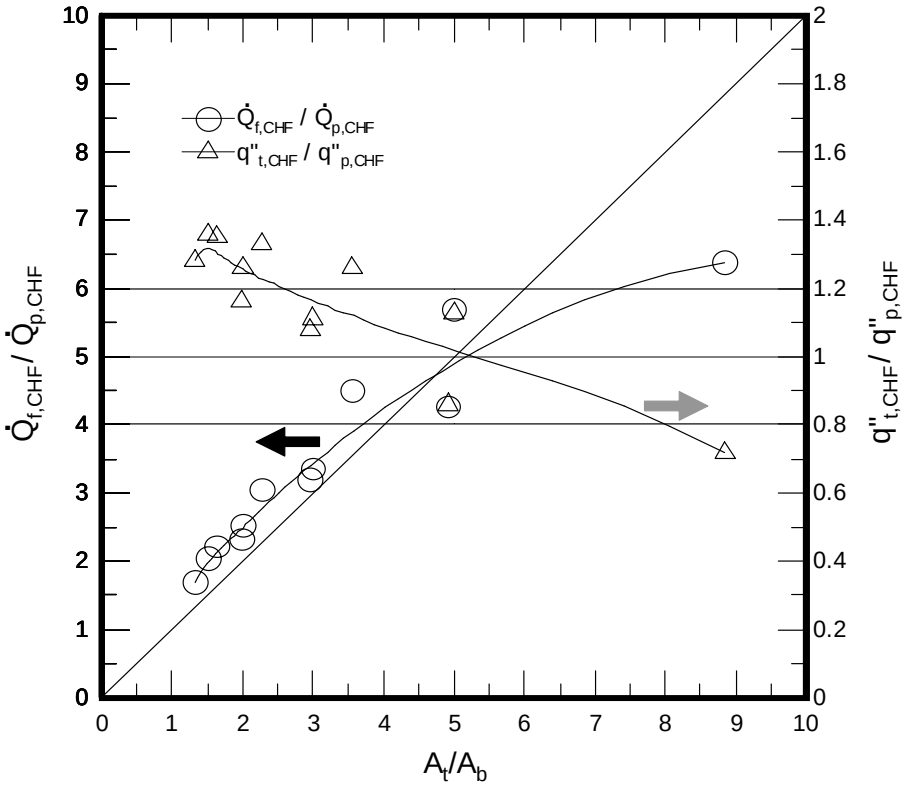

Figure 5.9 Enhancement of maximum heat rate and critical heat flux versus enhancement of area.

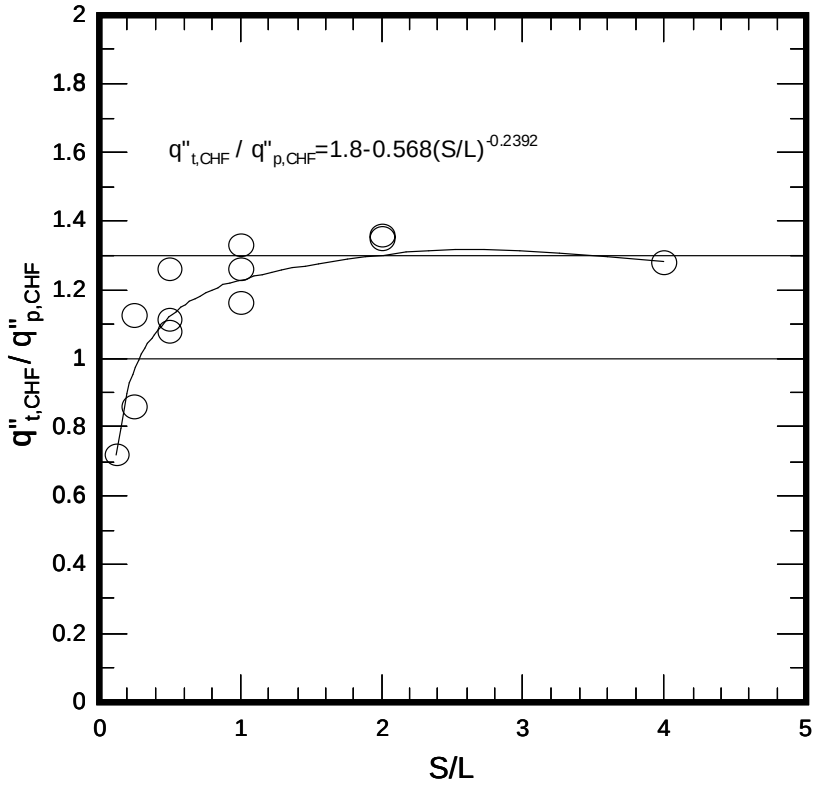

Figure 5.10 Normalized overall heat flux versus dimensionless parameter (S/L).

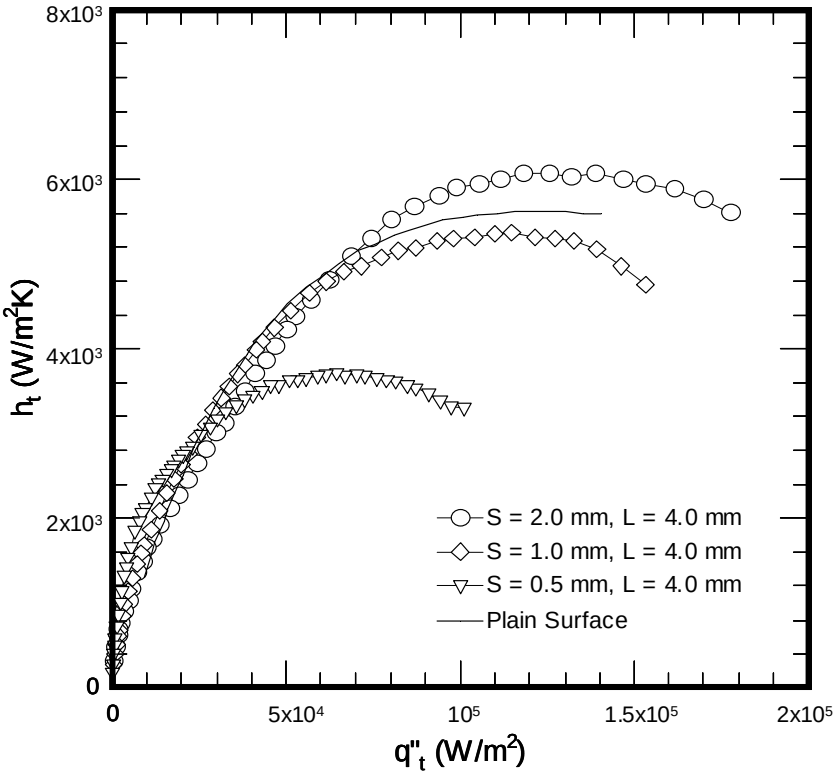

Figure 5.11 Effect of fin spacing on overall heat transfer coefficient on the mini-finned surfaces in vertical orientation (L=4.0mm, decreasing heat flux).

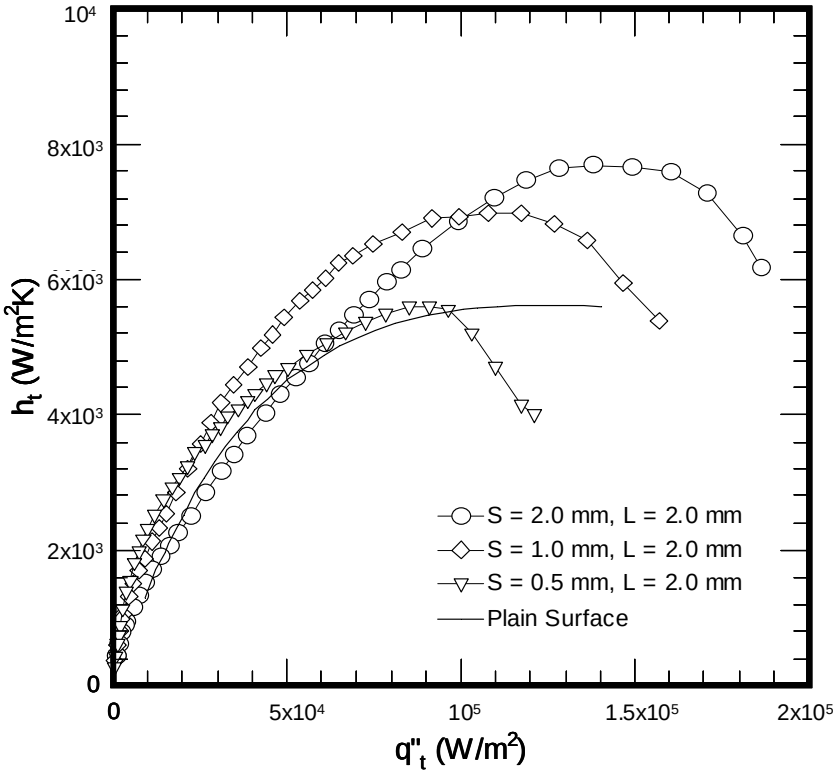

Figure 5.12 Effect of fin spacing on overall heat transfer coefficient on the mini-finned surfaces in vertical orientation (L=2.0mm, decreasing heat flux).

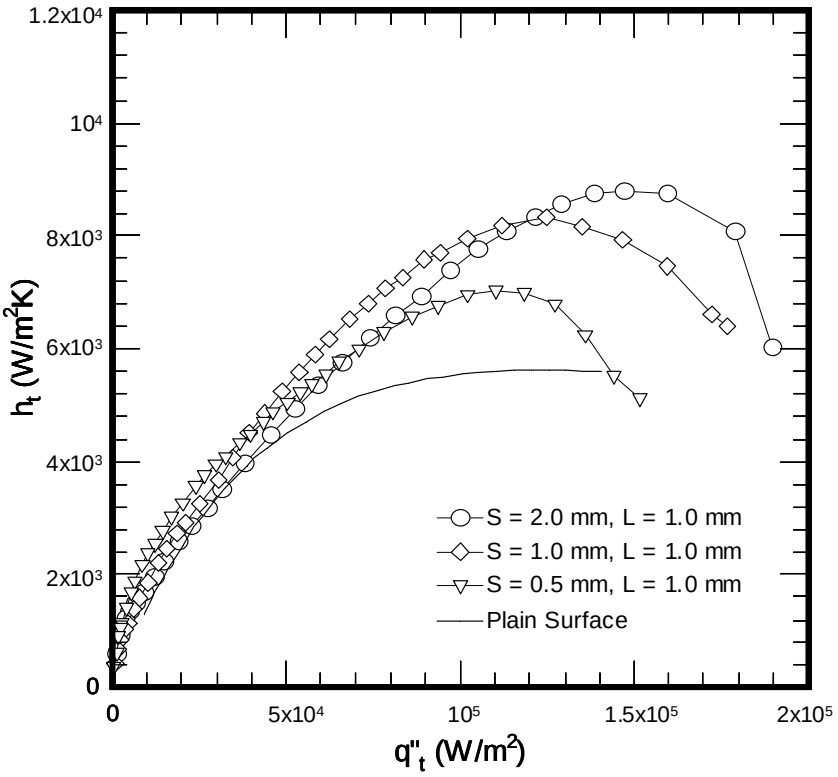

Figure 5.13 Effect of fin spacing on overall heat transfer coefficient on the mini-finned surfaces in vertical orientation (L=1.0mm, decreasing heat flux).

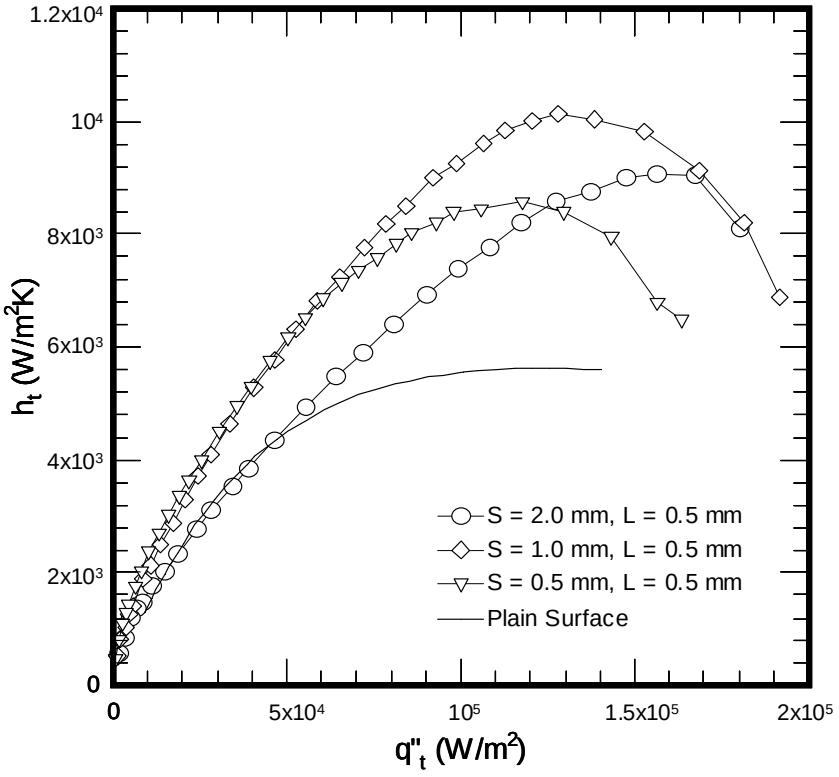

Figure 5.14 Effect of fin spacing on overall heat transfer coefficient on the mini-finned surfaces in vertical orientation (L=0.5mm, decreasing heat flux).

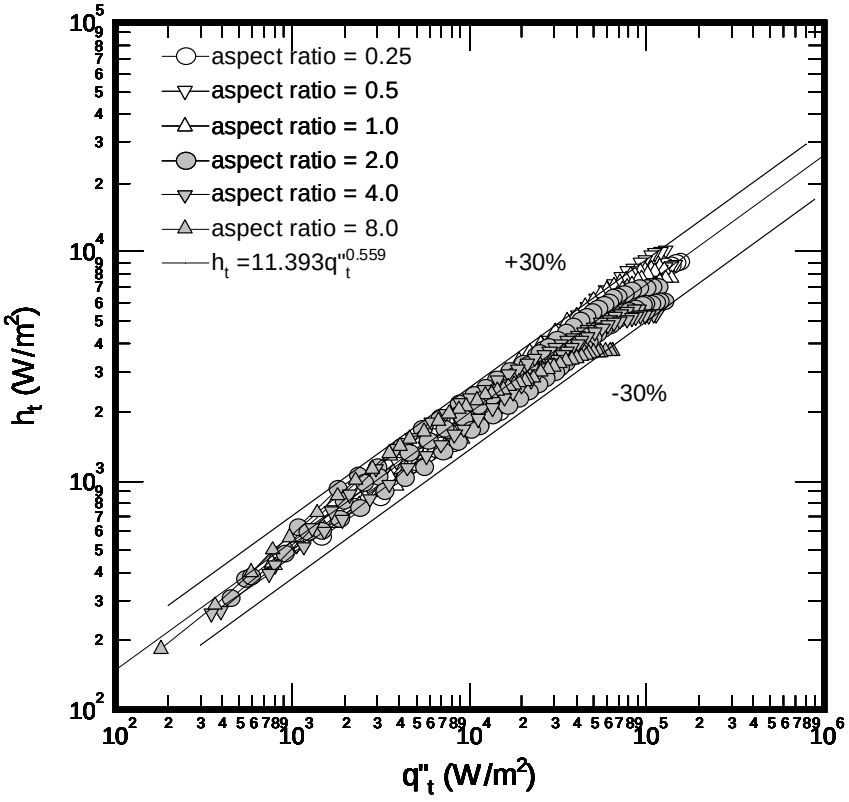

Figure 5.15 Overall heat transfer coefficients versus overall heat flux for different finned surfaces in vertical orientation.

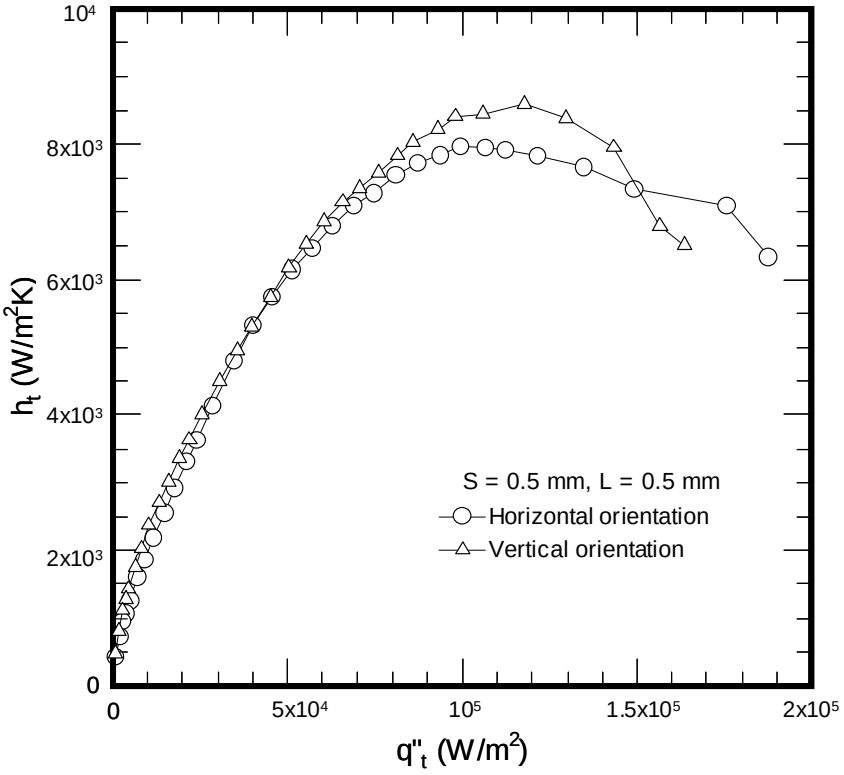

Figure 5.16 Orientation effect to denser mini-finned surface with and 0.5mm fin length.

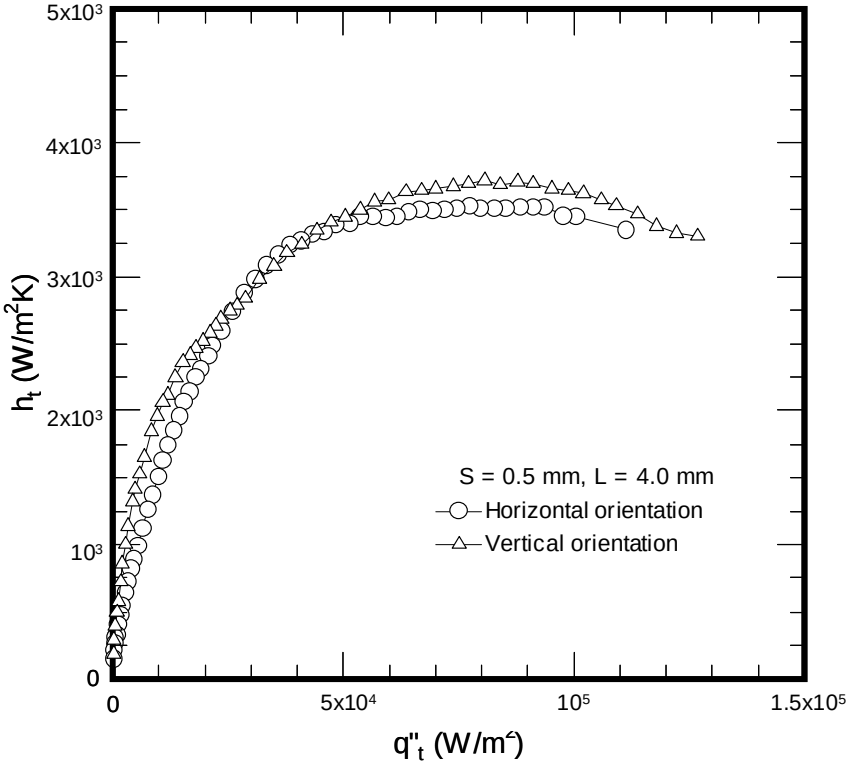

Figure 5.17 Orientation effect to denser mini-finned surface with 4.0mm fin length.

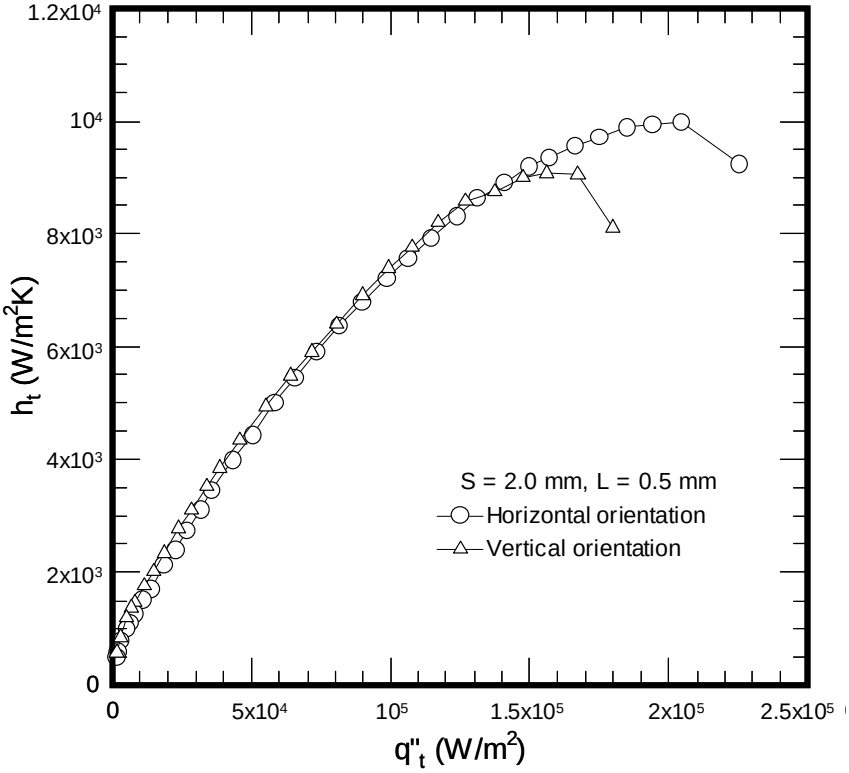

Figure 5.18 Orientation effect to rarer mini-finned surface with 0.5mm fin length.

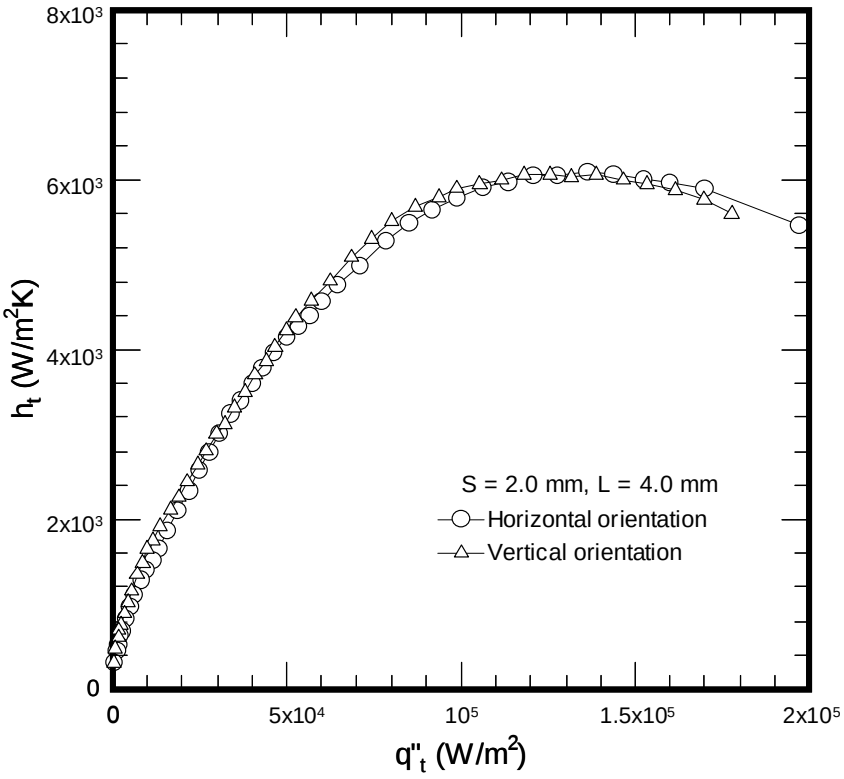

Figure 5.19 Orientation effect to rarer mini-finned surface with 4.0mm fin length.